ELSEVIER

Journal of Organometallic Chemistry 649 (2002) 147–151

Journal of Organometallic Chemistry

www.elsevier.com/locate/jorganchem

Coordination chemistry of tin
Part III. The crystal structure and thermal behavior of dipotassium dimethyl-tetrafluoro-stannate dihydrate, $K_2[(CH_3)_2SnF_4]\cdot 2H_2O$

Ibrahim Abdelhalim Ahmed [a], Guido Kastner [a], Hans Reuter [a,*], Dietrich Schultze [b]

[a] *Institut für Chemie-Anorganische Chemie, Universität Osnabrück, Barbarastraße 7, D-49069 Osnabruck, Germany*
[b] *BAM, Labor I.33 Röntgenstruktur- und Phasenanalyse, Rudower Chaussee 5, 12489 Berlin, Germany*

Received 7 May 2001; accepted 19 November 2001

Abstract

Reaction of $(CH_3)_2SnF_2$ with two equivalents of KF in aqueous medium leads to the formation of the complex salt $K_2[(CH_3)_2SnF_4]\cdot 2H_2O$ (**1**). Its crystal structure was determined by single-crystal X-ray diffraction. Complex **1** crystallizes in the monoclinic space group $C2$ (No. 5) with the lattice parameters $a = 9.265(1)$, $b = 7.556(1)$, $c = 7.076(1)$ Å; $\beta = 98.21(1)°$ and $Z = 2$. The structure is characterized by the anion $[(CH_3)_2SnF_4]^{2-}$ in which the tin atom adopts a slightly distorted octahedral coordination, with the methyl groups in *trans* position. The potassium cations are pentacoordinated from three fluorine atoms and the oxygen atoms of two water molecules in the form of a distorted square pyramid. In addition, the thermal behavior of the compound was studied with the aid of TG/DSC-measurements coupled with MS, revealing that the dehydration of **1** takes place at 75 °C, with an enthalpy of 57.79 kJ mol^{-1}, and that it decomposes without melting in two further endothermic steps to undetermined phases in the system $KF–SnF_2–SnF_4$ and free carbon ($\sim 0.1\%$).

Keywords: Tin; Crystal structures; NMR; DSC; MS

1. Introduction

Diorganotin difluorides, R_2SnF_2, are known since a long time [1]. They are believed to have polymeric structures with an octahedral environment around tin because — in comparison with the corresponding chloride, bromide and iodide solids — they are solids that melt or decompose at higher temperatures and are only slightly soluble in indifferent organic solvents. This suggestion was confirmed by Schlemper and Hamilton [2] in 1966, when they determined the crystal structure of Me_2SnF_2. In the solid state, this difluoride consists of an infinite two-dimensional network of edge-sharing $\{Me_2SnF_{4/2}\}$-octahedra with linear fluorine bridges and the methyl groups in *trans* position.

Among the chemical reactions of the diorganotin difluorides, those with an excess of fluoride ions are of special interest because the addition products formed open a wide field for the preparation of diorganotin fluoro-complexes. The first example of such an addition product, the compound $K_2[Et_2SnF_4]$, was prepared by Krause [3] in 1917. His formulation, $Et_2SnF_2\cdot 2KF$, was in accordance with Pfeiffer's earlier contribution to the theory of double salts [4]. An X-ray diffraction analysis was performed [5] with an analogous compound, $[NH_4]_2[Me_2SnF_4]$, which reveals that it consists of isolated $[Me_2SnF_4]^{2-}$ octahedra, again with the organic ligands in a *trans* position. In addition to these anhydrous adducts, there is also a hydrated form known, $K_2[Me_2SnF_4]\cdot 2H_2O$, first described by Wilkins and Haendler [6] in 1965.

Later on, a second class of addition products was found. In the compound $[Et_4N][Me_4Sn_2F_5]$ [7], there exists a polymeric three-dimensional network of $[Me_2Sn_2F_3]^-$ anions interconnected to each other by

* Corresponding author. Tel.: +49-541-969-2778; fax: +49-541-969-3323.
E-mail address: hreuter@rz.uni-osnabrueck.de (H. Reuter).

0022-328X/02/$ - see front matter
PII: S0022-328X(02)01111-7

angled fluorine bridges. Again, the tin atoms exhibit an octahedral geometry, with the methyl groups *trans* to each other.

Here, we present the single-structure determination of the adduct $K_2[Me_2SnF_4]\cdot 2H_2O$ as well as its thermal behavior.

2. Experimental

2.1. Preparation

Compound **1** was prepared by the method of Wilkins and Haendler [6]. All reagents were purchased from Fluka and used without further purification. Colorless crystals of **1** were grown through slow evaporation of an aqueous solution at room temperature (r.t.).

2.2. Crystal structure

Colorless, plate-like single crystals were obtained after recrystallization from H_2O. A species of dimension $0.46 \times 0.31 \times 0.09$ mm, suitable for X-ray diffraction analysis, was chosen using a polarization microscope and fixed at the top of a glass thread with epoxy resin.

Table 1
Crystal data and structure refinement parameters for $K_2[Me_2SnF_4]\cdot 2H_2O$ (**1**)

Empirical formula	$C_2H_{10}F_4K_2O_2Sn$
Formula weight	338.99 g mol^{-1}
Temperature (K)	293(2)
Wavelength (Å)	0.71073
Crystal system	Monoclinic
Space group	$C2$
Unit cell dimensions	
a (Å)	9.2747(18)
b (Å)	7.5658(10)
c (Å)	7.0806(10)
β (°)	98.231(12)
V (Å^3)	491.73(13)
Z	2
D_{calc} (g cm^{-3})	2.289
Absorption coefficient (mm^{-1})	3.461
$F(000)$	324
Theta range for data collection (°)	2.91–28.00
Index ranges	$-12 \le h \le 12$, $-9 \le k \le 9$, $-9 \le l \le 9$
Reflections collected	1332
Independent reflections	1184 [$R_{int} = 0.0332$]
Completeness to $\theta = 28.00°$	100%
Absorption correction	Empirical from psi-scans
Max/min transmission	0.8557, 0.6980
Refinement method	Full-matrix least-squares on F^2
Data/restraints/parameters	1184/1/56
Final R indices [$I > 2\sigma(I)$]	$R_1 = 0.0233$, $wR_2 = 0.0599$
R indices (all data)	$R_1 = 0.0233$, $wR_2 = 0.0599$
Goodness-of-fit on F^2	1.104
Extinction coefficient	0.0147(12)
Largest difference peak and hole (e Å^3)	1.154 and -0.600

The crystallographic measurements were performed on a Siemens P4 four-circle diffractometer with Mo–K_α radiation and a graphite monochromator at r.t., using the program package XSCANS [8]. Unit cell parameters were derived by least-squares refinement of the angle settings of 42 arbitrarily found reflections in the range $16.25° < \theta < 34.36°$. Reflection intensities were collected within two octants ($-h-kl$, $-h-k-l$) until $2\theta = 56°$. No intensity decay was observed.

Dipotassium dimethyl-tetrafluoro-stannate dihydrate, **1**, crystallizes in monoclinic form, with $a = 9.265(1)$, $b = 7.556(1)$, $c = 7.076(1)$ Å; $\beta = 98.21(1)°$, $V = 490.2$ Å^3 and $Z = 2$. Because the systematic absences (hkl only present for $h + k = 2n$, $h01$ only present for $h = 2n$ and $0k0$ only present for $k = 2n$) found in the data set were consistent with the three possible space groups, $C2$, Cm and $C2/m$, all of them were checked for structure solution and refinement. Only by applying the symmetry operations of $C2$ (No. 5 [9]), a chemically meaningful structure model with acceptable R values and thermal displacement parameters for the individual atoms was obtained. The resulting Flack parameter, however, indicated the presence of racemic twinning. The correct selection of the non-centrosymmetric space group was confirmed by measuring a small SHG effect.

The structure was solved by direct methods and refined by full-matrix least-squares calculations (on F^2) of the SHELXTL program package [10]. All non-H atoms were refined anisotropically. The H atoms were placed in geometrically calculated positions, using a riding model, and refined with a common isotropic displacement parameter. Further crystallographic data, details of the data collection and structure determination are given in Table 1; characteristic bond lengths and angles are given in Table 2. Figures were drawn using ORTEP-3 [11].

2.3. Spectroscopic measurements

IR data (4000–400 cm^{-1}) were collected in a Bruker vector 22 FT spectrometer. ^{1}H- and ^{13}C{^{1}H}-NMR spectra were recorded in D_2O, using a Bruker Advance DPX-250 spectrometer; ^{19}F-NMR spectra were obtained in a Bruker-ARX-400 spectrometer.

IR (cm^{-1}, KBr): 3425 br, 3000 m, 2927 m, 2802 w, 2382 vw, 1731 vw, 1681 w, 1509 vw, 1416 w, 1195 m, 777 s-br, 581 s, 519 w, 485 w (also see Refs. [8,9]). ^{1}H-NMR (250 MHz, TMS_{int}, ppm): δ 0.57 (s, CH_3), $^2J(^1H-^{119/117}Sn = 103.0/98.8$ Hz), 4.71 (s, H_2O). ^{13}C-NMR (63 MHz, ppm): δ 6.85 (s), $^1J(^{13}C-^{119/117}Sn = 979.6/937.0$ Hz). ^{19}F-NMR (376.47 MHz, ppm): δ -121.63 (s), $^1J(^{19}F-^{119/117}Sn =$ not observed).

Table 2
Selected bond lengths (Å) and bond angles (°) for **1**

Bond lengths			
Sn(1)–C(1)	2.111(3)	K(1)–F(1) # 2	2.617(2)
Sn(1)–C(1) # 1	2.111(3)	K(1)–F(2) # 3	2.595(12)
Sn(1)–F(1)	2.135(2)	K(1)–F(3)	2.603(11)
Sn(1)–F(1) # 1	2.135(2)	K(1)–O(1)	2.825(12)
Sn(1)–F(2)	2.064(14)	K(1)–O(2)	2.736(12)
Sn(1)–F(3)	2.109(12)		
Bond angles			
C(1)–Sn(1)–C(1) # 1	178.9(7)	F(1) # 6–K(1)–O(1)	117.1(3)
C(1)–Sn(1)–F(1)	90.9(1)	F(1) # 6–K(1)–O(2)	119.6(3)
C(1)–Sn(1)–F(2)	90.6(4)	F(2) # 5–K(1)–F(3)	81.5(1)
C(1)–Sn(1)–F(3)	89.4(4)	F(2) # 5–K(1)–O(1)	137.2(1)
C(1) # 1–Sn(1)–F(1)	89.1(1)	F(2) # 5–K(1)–O(2)	83.2(4)
F(1)–Sn(1)–F(1) # 1	179.2(7)	F(3)–K(1)–O(1)	81.5(3)
F(1)–Sn(1)–F(3)	90.4(3)	F(3)–K(1)–O(2)	136.5(1)
F(2)–Sn(1)–F(1)	89.6(3)	O(1)–K(1)–O(2)	82.8(1)
F(2)–Sn(1)–F(3)	180.0	K(1) # 3–F(2)–K(1) # 4	98.7(6)
Sn(1)–F(1)–K(1) # 2	130.1(1)	K(1)–F(3)–K(1) # 1	98.3(5)
Sn(1)–F(2)–K(1) # 3	130.6(3)	K(1)–O(1)–K(1) # 7	95.1(5)
Sn(1)–F(3)–K(1)	130.8(3)	K(1) # 7–O(2)–K(1)	99.3(6)
F(1) # 6–K(1)–F(3)	103.6(3)		
F(1) # 6–K(1)–F(2) # 5	105.0(3)		

Symmetry transformations used to generate equivalent atoms: # 1, $-x+1$, y, $-z+1$; # 2, $-x+3/2$, $y+1/2$, $-z+1$; # 3, x, $y+1$, z; # 4, $-x+1$, $y+1$, $-z+1$; # 5, x, $y-1$, z; # 6, $-x+3/2$, $y-1/2$, $-z+1$; # 7, $-x+1$, y, $-z+2$.

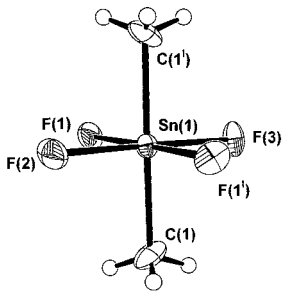

Fig. 1. Perspective view of the slightly distorted octahedral $\{Me_2SnF_4\}^{2-}$-ion in the crystal structure of **1**, with the atomic numbering scheme used; atoms are drawn as thermal displacement ellipsoids showing the 50% probability level; hydrogen atoms are drawn as spheres with arbitrary radii.

2.4. Thermal measurements

Differential scanning calorimetry (DSC) was carried out with a Labsys™ (TG-DSC/DTA) calorimeter from Setaram. The heat flow rate was 5 °C min^{-1}. Calibration of temperature and enthalpy was performed with melting points and enthalpies of indium, bismuth and lead [12,13]. The thermodynamic data were determined by integration of the DSC signals. In addition, measurements were performed with a Setaram thermobalance TAG 24 with simultaneous DTA and coupled with mass spectroscopic gas analysis (Balzer Thermostar). Samples of about 15 mg were pressed into ceramic crucibles and introduced into the apparatus, which was then evacuated and filled with pure argon. The measurements were performed in a N_2 stream with heating and cooling rates of 5 K min^{-1}.

Stepwise degradation; selected MS signals in order of decreasing ion-currents, 1st step, $T_{onset} = 75$ °C: H_2O ($m/e = 18$), OH ($m/e = 17$); 2nd step, $T_{onset} = 275$ °C: Me_3Sn ($m/e = 161$, 163, 165), CH_3 ($m/e = 15$); MeSn ($m/e = 131$, 133, 135), Me_2Sn ($m/e = 146$, 148, 150), Sn ($m/e = 116$, 118, 120), Me_2SnF ($m/e = 165$, 167, 169), SnF ($m/e = 135$, 137, 139), MeSnF ($m/e = 150$, 152, 154), SnF_2 ($m/e = 154$, 156, 158), $MeSnF_2$ ($m/e = 169$, 171, 173), Me_3SnF ($m/e = 180$, 182, 184), Me_4Sn ($m/e = 176$, 178, 180), Me_2SnF_2 ($m/e = 184$, 186, 188), SnF_3 ($m/e = 175$); $MeSnF_3$ ($m/e = 188$, 190, 192), SnF_4 ($m/e = 192$, 194, 196); 3rd step, $T_{onset} = 370/396$ °C: CH_4 ($m/e = 16$), CH_3, Me_3Sn, MeSn, Me_2Sn, Sn, Me_2SnF, Me_3SnF, MeSnF, SnF, Me_2SnF_2, SnF_2, $MeSnF_2$, Me_4Sn, $MeSnF_3$, SnF_4.

3. Results and discussion

3.1. Crystal structure

The asymmetric unit of the crystal structure consists of one tin atom and two fluorine and two oxygen atoms in special positions, all on twofold axes. A third fluorine atom as well as a carbon atom and a potassium cation are placed in general positions. The formation of $\{Me_2SnF_4\}^-$ anions with slightly distorted octahedral geometry results from this (Fig. 1). Within these anions, the methyl groups occupy a *trans* position (174.9°), as predicted by Wilkins and Haendler [6].

The Sn–C bond length of 211.1 pm is nearly identical with the tin–carbon bond lengths found in $(NH_4)_2[(CH_3)_2SnF_4]$ (an average of 210.9 pm) [5] and $(Et_4N)[(CH_3)_4Sn_2F_5]$ (an average of 211.1 pm) [7]. Within **1**, the four tin–fluorine bond lengths show great differences. Two of them (F1)/(F3) lie in the range 213.5–210.9 pm, with a mean value of 212.2 pm, whereas the third one (F2) is significantly shorter (206.4 pm). The average of 210.3 pm over all three values is greater than the value given by Reuter and Puff [14] for a 'normal' tin–fluorine bond, an effect that can be attributed to the higher coordination number of the central tin atom and to the bridging function of the fluorine atoms.

As can be seen from Fig. 2, the potassium atom is fivefold-coordinated from three fluorine atoms and the oxygen atoms of the two water molecules. The potassium–oxygen bond lengths are 282.5 and 276.3 pm, respectively, with a bond angle of 82.8°. The potassium–fluorine distances are in the range 259.5–261.7 pm, with an average of 260.6 pm. The bond angles (see Table 2) between the F^-, K^+ and H_2O result in a

distorted square-pyramidal coordination of the potassium ion, with an apical fluorine atom and two basal oxygen and fluorine atoms. Because the water molecules and the basal fluorine atoms bridge two potassium ions, the square-pyramidal building units are connected to each other within their basal plane, forming slightly curved chains parallel to the *c*-axis of the unit cell. With the top of the square pyramid above and below their basis, these $\{KO_{2/2}F_{2/2}F\}$-chains remind very much of the planes of the square-pyramidal $\{SnO_{4/2}O\}$-building units found in the crystal structure of SnO [15].

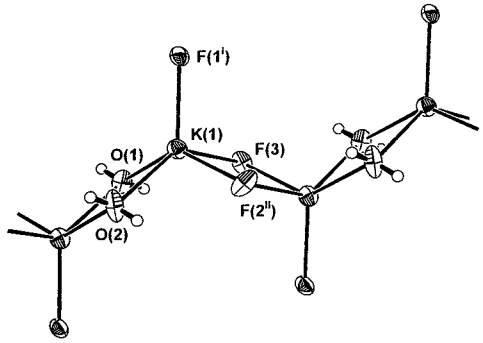

Fig. 2. Detail of the crystal structure of $K_2[Me_2SnF_4]\cdot 2H_2O$, showing the chain of square-pyramidal $\{KO_{2/2}F_{2/2}F\}$-units propagating along the crystallographic *c*-axis.

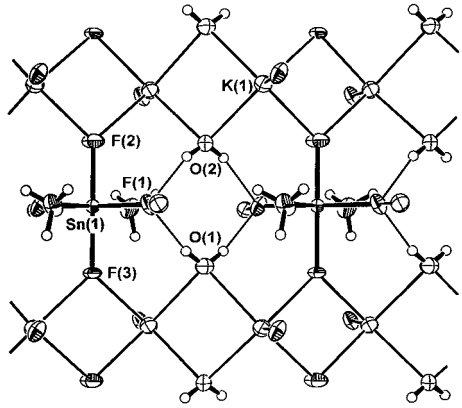

Fig. 3. Structure of a sheet within the crystal structure of **1** formed from octahedral $\{Me_2SnF_4\}^{2-}$-ions and the chains of square-pyramidal $\{KO_{2/2}F_{2/2}F\}$-units. Each anion connects two cation chains within the same sheet, giving rise to a series of two pairs of strong O–H···F hydrogen bonds between water molecules and anions. The corresponding fluorine atoms occupy the apical position in two $\{KO_{2/2}F_{2/2}F\}$-units lying below and above the sheet shown, thus forming a three-dimensional network.

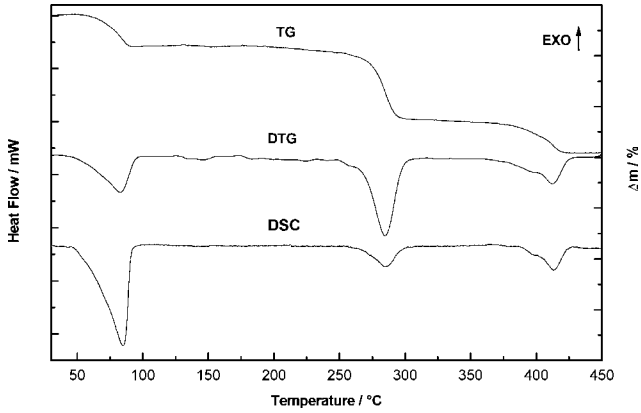

Fig. 4. General view of the thermal behavior of **1**, showing the changes in the TG, DTG and DSC curves with rising temperature. Details and data are explained in the text.

Within the *bc*-plane (Fig. 3) of the unit cell, the chains of these $\{KO_{2/2}F_{2/2}F\}$-units are interconnected by the anions, thus forming layers and giving rise to the formation of strong OH···F-hydrogen bonds with O···F distances of 275 and 278 pm and O–H···F angles of 165.2 and 161.1°, respectively. The two F-atoms involved in this hydrogen bond system occupy the apical position in two $\{KO_{2/2}F_{2/2}F\}$-units lying below and above the $\{Me_2SnF_4\}^-$ anion, so that all in all, a three-dimensional network results.

3.2. Thermal behavior

During thermal treatment, $K_2[Me_2SnF_4]\cdot 2H_2O$ shows a stepwise loss of mass, accompanied with three endothermic effects (see Fig. 4). The first and second effects occur at $T_{onset} = 75$ °C ($T_{top\text{-}of\text{-}peak} = 106$ °C), with $\Delta H = 57.79$ kJ mol^{-1}, and $T_{onset} = 275$ °C ($T_{top\text{-}of\text{-}peak} = 295$ °C), with $\Delta H = 10.28$ kJ mol^{-1}. Whereas the third effect splits into two peaks at $T_{onset} = 370$ °C ($T_{top\text{-}of\text{-}peak} = 378$ °C) and $T_{onset} = 396$ °C ($T_{top\text{-}of\text{-}peak} = 415$ °C), with $\Delta H = 11.39$ kJ mol^{-1} (sum of both peaks). The weight losses are 6.4, 14.3 and 6.2%, respectively.

During the first endothermic effect, in the mass spectrometer, maxima are observed for $m/e = 18$ (H_2O) and $m/e = 17$ (OH), with an ion current ratio of 5:1. As expected, this indicates the evolution of water as a result of the dehydration process of the compound. However, the weight loss of 6.4% is appreciably smaller than the expected value of 10.6%. We suggest that this discrepancy results from the grinding of the probe during its preparation for thermal analysis.

The interpretation of the degradation process during the two effects that follow is more difficult because tin possesses a lot of stable isotopes. In the following study, especially species with ^{118}Sn were considered for explanation. During the second phase of degradation, the main volatile products are Me_3Sn, with $m/e = 161$, 163 and 165, and CH_3, with $m/e = 15$. Furthermore, species like MeSn, Me_2Sn, Sn, Me_2SnF, SnF, MeSnF, SnF_2, $MeSnF_2$, Me_3SnF, Me_4Sn, Me_2SnF_2, SnF_3, $MeSnF_3$ and SnF_4 are evolved (for m/e also see Section 2). The ion currents of all these signals are located parallel to each other and decrease to three exponentials in the ions–current with respect to the order

mentioned. This indicates that these species come from the same reaction. However, most of these species are radicals, which cannot be formed as the primary volatile products of the thermal degradation of the compound but by fragmentation of a few volatile products within the mass spectrometer. The high concentration of CH_3 found made us suggest that this species is the main fragmentation product and that Me_4Sn is the first volatile product of degradation. Because of the lack of the MS signal of F ($m/e = 19$), we exclude that Me_3SnF is formed as the main product. Nevertheless, it may be formed as a side product, as can be seen from the other fluorine-containing species observed.

The splitting in the third endothermic effect, which is seen on the TG, DTG and DSC curves is not found in the mass spectrometer. Herein, mainly the same species as in the second effect are observed, with the remarkable difference that now CH_4 shows the strongest ion-current. In our opinion, the formation of CH_4 most probably results from a degradation reaction of Me_4Sn corresponding to the equation: $(CH_3)_4Sn \rightarrow 3CH_4 + Sn + C$. However, after repetitions of cooling and heating cycles of the black–gray residue, no evidence for the presence of metallic tin was found (absence of melting peak of tin on the DSC curve). This means that this residue is composed from phases in the system $KF–SnF_2–SnF_4$ and free carbon ($\sim 0.1\%$).

4. Supplementary material

Crystallographic data for the structural analysis have been deposited with the Cambridge Crystallographic Data Centre, CCDC no. 173831 for compound **1**. Copies of this information may be obtained free of charge from The Director, CCDC, 12 Union Road, Cambridge CB2 1EZ, UK (Fax: +44-1223-336033; e-mail: deposit@ccdc.cam.ac.uk or www: http://www.ccdc.cam.ac.uk).

Acknowledgements

We are grateful to Dr K. Betzler, Dr A. Hepp, Mrs K. Ruecker and to the 'Fonds der chemischen Industrie' for financial support.

References

[1] (a) E. Krause, A.v. Grosse, Die 1 Chemie der metall-organischen Verbindungen, Borntraeger, Berlin, 1937;
(b) Gmelin Handbuch der Anorganischen Chemie, Tin, Part 5, Organotin Fluorides, Diorganotin Difluorides, Springer, Berlin, 1978;
(c) P.G. Harrison, The Chemistry of Tin, Blackie, Chapman and Hall, USA, 1989, p. 187 and references therein.
[2] E.O. Schlemper, W.C. Hamilton, Inorg. Chem. 5 (1966) 995.
[3] E. Krause, Ber. Dtsch. Chem. Ges. 51 (1918) 1447.
[4] P. Pfeiffer, Liebigs Ann. Chem. 376 (1910) 310.
[5] D. Tudela, J. Organomet. Chem. 471 (1994) 63.
[6] C.J. Wilkins, H.M. Haendler, J. Chem. Soc. (1965) 3174.
[7] T.H. Lambertsen, P.G. Jones, R. Schmutzler, Polyhedron 11 (1992) 331.
[8] XSCANS Programm zur Steuerung des Siemens P4-Vierkreisdiffraktometers, Version 2.1, Siemens, 1994.
[9] T. Hahn (Ed.), International Tables for Crystallography, Kluver, Dordrecht, 1996.
[10] SHELXTL, Integrated System for the Determination of Crystal Structures from Diffraction Data, Release 5.03, Siemens, 1995.
[11] L.J. Farrugia, ORTEP-3 for Windows, J. Appl. Crystallogr. (1997) 565.
[12] J.O. Hill (Ed.), For Better Thermal Analysis and Calorimetry, ICTA, 1991.
[13] W.F. Hemminger, H.K. Cammenga, Methoden der thermischen Analyse, Springer, Berlin, 1989.
[14] H. Reuter, H. Puff, J. Organomet. Chem. 379 (1989) 223.
[15] J. Pannetier, G. Denes, Acta Crystallogr. Sect. B 36 (1980) 2763.